Analysis of Channel Addition/Removal Response in All-Optical Gain-Clamped Cascade of Lumped Raman Fiber Amplifiers

M. Karásek, J. Kaňka, and Jan Radil

***Abstract*—The effect of addition and/or dropping of wavelength-multiplexed channels in a network comprising three concatenated lumped Raman fiber amplifiers (LRFAs) have been analyzed by numerical simulation and verified experimentally. The first LRFA in the cascade is gain clamped using a ring-laser configuration, and the lasing power propagates through the cascade. A large-signal numerical model that incorporates time variation effects and the downstream propagation of signal, upstream propagation of pumps, and downstream and upstream propagation of amplified spontaneous emission spectral components has been used for the theoretical analysis. The LRFAs consist of 16 km of dispersion-compensating fiber counterdirectionally pumped at 1455 nm by a Raman fiber laser. Channel addition/removal is simulated by propagating through the cascade of LRFAs optical power from two laser diodes. One of them is square-wave modulated at 500 Hz, and power fluctuations of the second continuous-wave signal caused by the cross-gain saturation effect in LRFAs are monitored.**

***Index Terms*—Optical fiber amplifiers, Raman amplification, wavelength-division multiplexing (WDM).**

I. Introduction

IN TRANSPARENT reconfigurable multiwavelength lightwave networks, the number of wavelength channels passing through an erbium-doped fiber amplifier (EDFA) may vary due to, e.g., network reconfiguration or failure of a channel. Cross-gain saturation in fiber amplifiers will induce power transients in the surviving channels, which can cause severe service impairment. As fiber amplifiers saturate on a total power basis, channel addition/removal in a multiaccess network will tend to perturb signals at other wavelengths that share all or part of the route. Although this perturbation will generally be small in a single amplifier, it will grow rapidly along a cascade. The steady state and the transient channel addition/removal response must be minimized to avoid error bursts in the surviving channels.

Signal power transients in concatenated highly pumped, deeply saturated EDFAs have been studied [1]. Several techniques have been suggested to control the unwanted surviving channel power excursions in EDFAs [2]–[5]. One of the simplest schemes among them is the all-optical gain-clamping (AOGC) method in which lasing in an EDFA is allowed. The EDFA gain is clamped regardless of input signal level [6]–[9]. Performance degradation of AOGC EDFAs due to ring-laser relaxation oscillation has been studied in [10].

Similar gain transients have recently been observed in counter-directionally pumped Raman fiber amplifiers (RFAs) [11], [12]. They are caused by nonnegligible propagation time along the Raman fiber and by signal-to-pump and signal-to-signal interactions, which result in partial pump depletion. When the signal power changes abruptly, the leading edge of the signal wave depletes the counterpropagating pump so that the main body of the signal does not experience the same high gain as the signal front. Two control schemes widely accepted in EDFAs have so far been suggested and experimentally verified for suppression of power transients in RFA: fast pump power control [13], [14] and all-optical gain clamping [15]–[18]. The proportional–integral–derivative (PID) control circuit was implemented in the control scheme demonstrated in [13] to vary the counterdirectional pump power. The control signal was derived either from the surviving channel output power or from both the surviving and the total output power. When the control was off, Raman gain fluctuations of the surviving channel ranged from 0.35 to 1.2 dB as the drop/total ratios ranged from $4/8$ to $20/24$ in the distributed RFA. The control algorithm kept gain fluctuations of surviving channels $<\pm 0.06$ dB. The gain-clamped lumped Raman fiber amplifier (LRFA) reported in [16] exhibits a net gain of 10 dB with a gain variation of only 0.3 dB for signal input power ranging from -22.5 to 2.7 dBm. Elimination of steady-state surviving channel power fluctuations and suppression of power surges has been demonstrated. The dynamic behavior of a gain-clamped multiwavelength pumped discrete Raman amplifier cascade investigated theoretically by numerical simulation in [18] assumed that the gain of each amplifier is clamped through an optical feedback loop.

This paper presents the experimental and theoretical results of surviving channel protection in a cascade of three LRFAs. In contrast with theoretical results presented in [18], only the gain of the first amplifier is clamped using an optical feedback loop in the form of a ring laser. Lasing power generated in the AOGC LRFA is let to propagate through the next two LRFAs. Channel addition/removal is simulated in the experiments by propagating through the cascade of LRFAs optical power from two laser diodes. One of them is square-wave modulated at 500 Hz, and

Manuscript received March 3, 2004; revised June 3, 2004. This work was supported in part by the Grant Agency of the Academy of Sciences of Czech Republic under Project A2 067 202 and in part by the Grant Agency of the Czech Republic under Project 102/04/0773.

M. Karásek and J. Kaňka are with the Institute of Radio Engineering and Electronics (IREE), Academy of Sciences of the Czech Republic, 182 51 Prague 8, Czech Republic (e-mail: karasek@ure.cas.cz).

J. Radil is with CESNET a.l.e., 160 00 Prague, Czech Republic.

Digital Object Identifier 10.1109/JLT.2004.833529

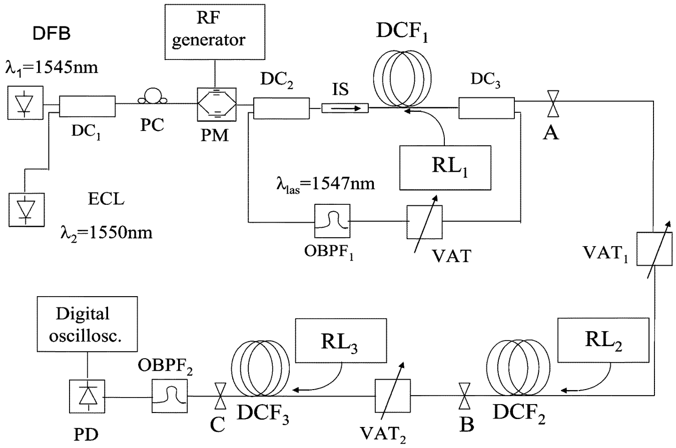

Fig. 1. Schematic diagram of the experimental setup of three AOGC LRFAs.

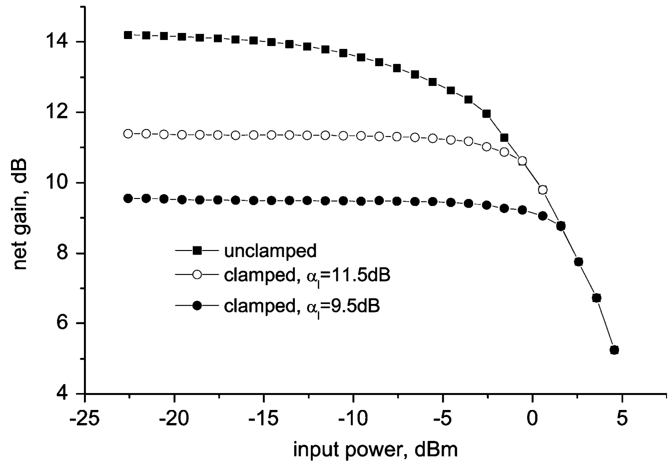

Fig. 2. Experiment: Single-channel (1545 nm) net gain of LRFA_1 as a function of input signal power with and without AOGC. Total loop loss α_l = 11.5 and 9.5 dB.

power fluctuations of the continuous-wave (CW) signal caused by the cross-gain saturation effect in the LRFA are monitored by a digital oscilloscope. The theoretical analysis is based on utilization of a large-signal numerical model that incorporates temporal properties and downstream propagation of multiple signals, upstream propagation of multiple pumps, and downstream and upstream propagation of amplified spontaneous emission (ASE) spectral components in the LRFA. Boundary conditions for propagation equations describing the AOGC LRFA have been modified to take into account the all-optical feedback loop. In contrast with the previously reported experiments and simulations of AOGC application to control the gain of LRFA, which were limited to a single amplifier [15]–[17], the analysis is extended on a cascade of three LRFAs. The AOGC LRFA and the other two LRFAs consist of 16 km of dispersion-compensating fiber (DCF) counterdirectionally pumped by a Raman fiber laser emitting at 1455 nm. The AOGC scheme of the first LRFA assumes the basic configuration in which automatic gain control is achieved by placing the LRFA in a ring- laser cavity to clamp its gain. It is demonstrated that when enough lasing is allowed, the AOGC can effectively suppress power fluctuations of surviving channels caused by the cross-gain saturation effect in all three LRFAs. The results imply that the AOGC cascade of the LRFA may find application in purely Raman amplified metropolitan area networks based either on DCF modules or on highly nonliner fiber modules.

II. Experimentation

A schematic representation of the experimental setup is shown in Fig. 1. Each of the three LRFAs consists of 16 km of DCF counterdirectionally pumped by 550 mW at 1455 nm from a high-power Raman fiber laser. When the pump power was increased above ≈600 mW, distributed Rayleigh reflections in the DCF resulted in gain instability and lasing action, which is described in [20]. Signals from a distributed feedback (DFB) laser and an internally modulated external-cavity laser (ECL) were combined in a 3-dB directional coupler (DC_1) and fed, via polarization controller (PC) and phase modulator (PM), to the cascade of three LRFAs. The signal of the DFB laser serves as a CW surviving channel to monitor output power fluctuations due to the cross-gain modulation in the LRFAs. The signal of the ECL was internally square-wave modulated at 500 Hz with a 50% duty cycle to simulate channel addition/removal. The wavelengths of the DFB laser and the ECL were $\lambda_1 = 1545$ nm and $\lambda_2 = 1550$ nm, respectively. The all-optical gain-controlled scheme used in the first LRFA of the cascade assumes the basic configuration in which automatic gain control is achieved by placing the amplifier in a ring-laser cavity to clamp its gain. To form the all-optical feedback loop, two conventional 70–30% directional couplers $(\mathrm{DC}_2$ and $\mathrm{DC}_3)$, an optical isolator (IS) suppressing the propagation of ASE^- in the ring resonator, and a 0.5-nm optical bandpass filter (OBPF) (OBPF_1) are used. The lasing wavelength of the AOGC LRFA_1 has been set at 1547 nm by the OBPF_1 and the lasing power adjusted by a variable attenuator (VAT). The lasing signal is let to propagate along the cascade together with the two signals at 1545 and 1550 nm. The experimentally obtained gain saturation characteristic of the amplifier is plotted in Fig. 2 for unclamped and two different clamped regimes. The gain was measured using light from the DFB laser source tuned at 1545 nm amplified by an EDFA (not shown in Fig. 1). The effect of stimulated Brillouin backscattering was suppressed by radio-frequency (RF) modulation of the light by electrooptical phase modulator. The OBPF_2 tuned at 1545 nm was placed at the output port of DC_3 (point A), and the gain was measured with a power meter. For the loop loss of $\alpha_l = 9.5$ dB, variation of net gain is <0.25 dB for a signal input power ranging from −22.5 to +0.25 dBm.

To measure the evolution of power transients of the 1545-nm signal along the cascade, the output spectrum from the AOGC LRFA_1 was attenuated by the variable attenuator VAT_1 and amplified by the second LRFA, the output spectrum of which was attenuated by VAT_2 and amplified by the third LRFA. Power fluctuations of the CW channel or of the lasing power were monitored using OBPF_2 and a digital sampling oscilloscope with optical head. Optical powers at the input to the directional coupler DC_2 were adjusted to −8 dBm (CW at 1545 nm) and −4 dBm (average power of the modulated signal at 1550 nm). In order to keep the average power level of the 1545-nm signal at

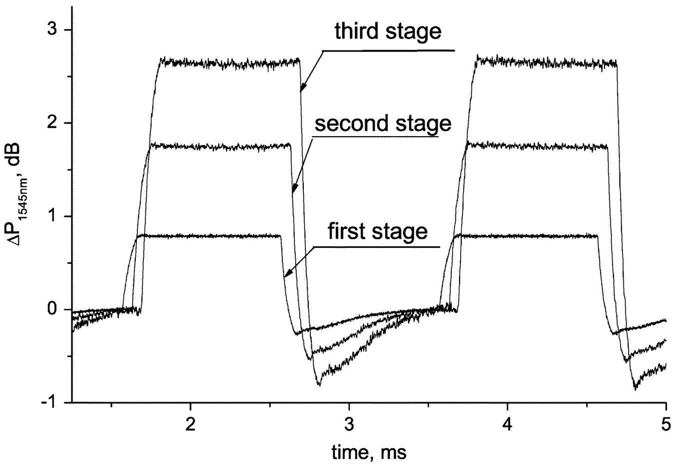

Fig. 3. Experiment: Output power variation of the 1545-nm signal at the output port of LRFA_1, LRFA_2, and LRFA_3 for the unclamped cascade.

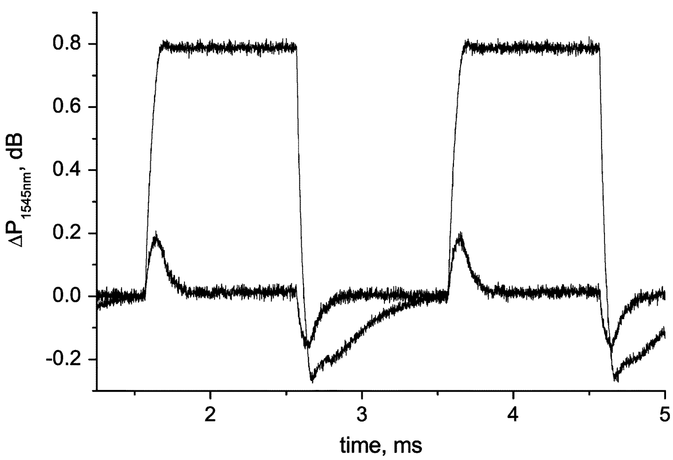

Fig. 4. Experiment: Output power variation of the 1545-nm signal at the output port of LRFA_1: comparison of the unclamped and clamped regime.

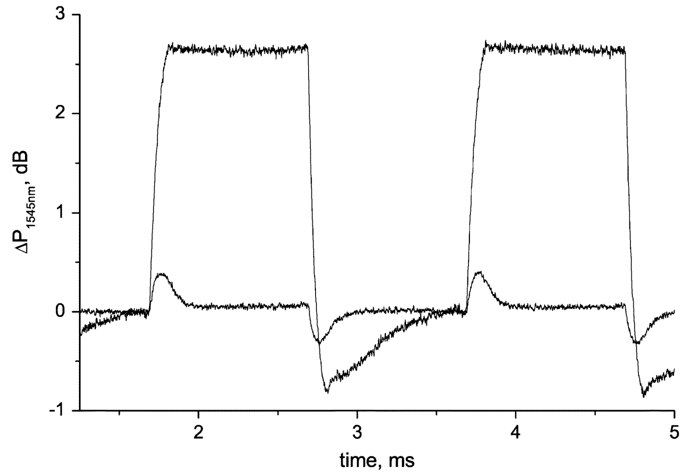

Fig. 5. Experiment: Output power variation of the 1545-nm signal at the output port of LRFA_3. Comparison of the unclamped and clamped regime.

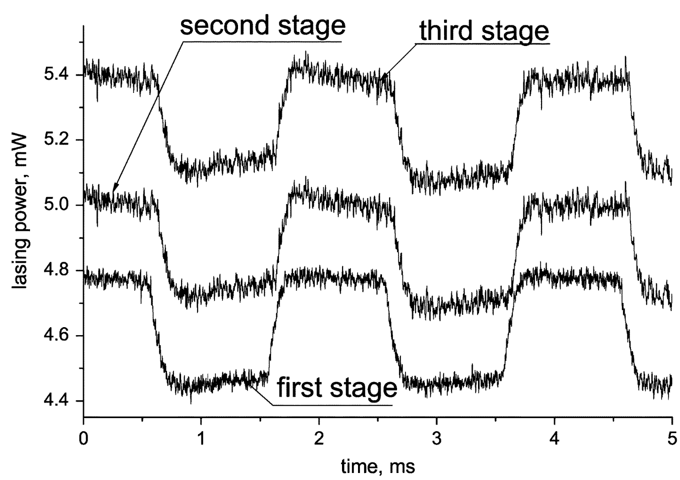

Fig. 6. Experiment: Time variation of the lasing power at 1547 nm recorded at the output of LRFA_1, LRFA_2, and LRFA_3.

the input port to the second and the third LRFA at -8 dBm, variable attenuators VAT_1 and VAT_2 were set to appropriate values $\beta_1 = 9.5$ dB and $\beta_2 = 14.2$ dB. The OBPF_2 and the oscilloscope with optical head were placed subsequently at the output port of LRFA_1, and LRFA_2, and LRFA_3 (points A, B, and C of Fig. 1), and the power transients were recorded with the optical feedback loop disconnected and closed.

Fig. 3 shows output power fluctuations of the 1545-nm channel for the unclamped regime (optical feedback loop disconnected) at the output port of LRFA_1, LRFA_2, and LRFA_3. The 1550-nm signal was switched off at $t = 1.5$ and 3.5 ms and on again at $t = 2.5$ and 4.5 ms. When the optical feedback loop of the AOGC LRFA_1 is closed, the lasing power of the ring laser compensates the power fluctuations of the square-wave-modulated signal at 1550 nm. Fig. 4 compares the time evolution of the 1545-nm signal at the output port of the AOGC LRFA_1 (point A) for the unclamped and clamped regime. It is seen that for $\alpha_l = 9.5$ dB, the steady-state fluctuation is fully eliminated. The power surge is six times lower, and the duration of power overshoots/undershoots that occur when the 1550-nm signal is switched OFF/ON is limited to 270 and 310 μs, respectively. As demonstrated in Fig. 5, suppression of power fluctuations at the output of LRFA_3 remains the same as at the output of LRFA_1. The time variation of the lasing power at 1547 nm at the output of individual LRFAs is shown in Fig. 6. It is seen that the lasing power that will be launched in the transmission fiber is about five times higher than the standard output power of commercial communication transmitters (0 dBm). When the lasing wavelength is close to signal channels and the link is composed of dispersion-shifted or nonzero-dispersion-shifted fiber, four-wave mixing between high power lasing and neighboring signal channels can have a detrimental impact on system performance.

III. Numerical Modeling

The model used for the simulation of the AOGC cascade of LRFAs is derived from the dynamic model of LRFA which was described in detail in [12] and follows the schematic diagram of our experimental setup of the cascade shown in Fig. 1. The numerical model of individual RLFA is based on the solution of partial differential equations describing propagation of pumps, signals, and both the downstream and upstream propagating ASE powers in each LRFA of the cascade. When backward Rayleigh scattering, temperature-dependent spontaneous Raman emission, and wavelength dependence of fiber loss and group velocity are taken into consideration, the propagation equations for forward- and backward-propagating pumps, signals, and spectral components of ASE powers $P^{+}(z,t,\nu), P^{-}(z,t,\nu)$ describing their evolution in space and time acquire the form [19] in (1) shown at the bottom of the page, where $V_g(\nu)$ is the frequency-dependent group velocity, $\alpha(\nu)$ the fiber background loss, $\gamma(\nu)$ the Rayleigh backscattering coefficient, $g_R(\nu-\mu)$ the Raman gain coefficient between waves with frequency ν, $\mu, K_{\rm eff}$ the polarization factor between pumps and Stokes signals, $A_{\rm eff}$ the effective interaction area of the fiber, h the Planck's constant, k the Boltzman's constant, and T the absolute temperature of the fiber.

For the steady-state solution of (1), we used an iterative procedure based on application of the fourth-order Runge–Kutta subroutine. The iteration is started with a forward integration of signals and forward-propagating ASE spectral components $P_s^{+}(z,\nu_s)$ and $P_{\rm ASE}^{+}(z,\xi)$. The backward pumps and backward ASE powers $P_p^{-}(z,\nu_p)$ and $P_{\rm ASE}^{-}(z,\xi)$ are set to zero. At each backward integration, the results of the previous forward integration $P_s^{+}(z,\nu_s)$ and $P_{\rm ASE}^{+}(z,\xi)$, together with the boundary conditions for backward pump and backward ASE powers, are used. Similarly, the results of the previous backward integration $P_p^{-}(z,\nu_p)$ and $P_{\rm ASE}^{-}(z,\xi)$, together with the boundary conditions for signal channels and forward ASE, are used. Boundary conditions reflect the introduction of the optical feedback loop. Boundary conditions for signal, pump, and ASE powers depend on the position of the amplifier in the cascade (subscript i) (see (2) at the bottom of the page). Here, $P_{s0}^{+}(\nu_s,t)$ is the time variable signal power at the input of the AOGC $\rm LRFA_1$ DCF fiber (equal for each channel ν_s), $P_{p0,i}^{-}$ is the counterdirectional pump power, L_i is the DCF length, β_1 and β_2 are the insertion loss of variable attenuators $\rm VAT_1$ and $\rm VAT_2$, $C_{\rm in}$ and $C_{\rm out}$ are the coupling ratios of the input and output couplers $\rm DC_1$ and $\rm DC_2$, $\alpha_{\rm is}$ and α_{va} represent the isolation of the optical isolator (IS) and the loss of the variable attenuator VAT, and $F(\nu)$ represents the transmissivity function of the optical bandpass filter $\rm OBPF_1$. The iteration process is stopped when, during two successive forward integrations, the gain of a selected signal channel does not change by more than 0.05%. Due to the optical feedback loop in the AOGC $\rm LRFA_1$, lasing power nucleates during the repeated forward and backward integration from the downstream ASE spectrum at the wavelength determined by $\rm OBPF_1$. Spectral components of downstream and upstream ASE power are calculated in the range from 1480 to 1620 nm with 1-nm resolution, unless otherwise stated. Depending on

$$
\begin{aligned}
\frac{\partial P^{\pm}(z,t,\nu)}{\partial z} \mp \frac{1}{V_g(\nu)}\frac{\partial P^{\pm}(z,t,\nu)}{\partial t} =& \mp \alpha(\nu)P^{\pm}(z,t,\nu) \pm \gamma(\nu)P^{\mp}(z,t,\nu)\\
&\pm P^{\pm}(z,t,\nu)\cdot\sum_{\xi>\nu}\frac{g_R(\nu-\xi)}{K_{\rm eff}A_{\rm eff}}[P^{\pm}(z,t,\xi)+P^{\mp}(z,t,\xi)]\\
&\pm h\nu\sum_{\xi>\nu}\frac{g_R(\nu-\xi)}{A_{\rm eff}}\cdot[P^{\pm}(z,t,\xi)+P^{\mp}(z,t,\xi)]\left[1+\frac{1}{e^{h(\xi-\nu)/kT}-1}\right]\Delta\nu\\
&\mp P^{\pm}(z,t,\nu)\cdot\sum_{\xi<\nu}\frac{\nu}{\xi}\frac{g_R(\nu-\xi)}{K_{\rm eff}A_{\rm eff}}[P^{\pm}(z,t,\xi)+P^{\mp}(z,t,\xi)]\\
&\mp 2h\nu P^{\pm}(z,t,\nu)\cdot\sum_{\xi<\nu}\frac{g_R(\nu-\xi)}{A_{\rm eff}}\left[1+\frac{1}{e^{h(\nu-\xi)/kT}-1}\right]\Delta\nu \qquad (1)
\end{aligned}
$$

$$
\begin{aligned}
P_{s,i}^{+}(z=0,\nu_s,t) &= \begin{cases} P_{s0}^{+}(\nu_s,t) & \dots\ \text{for } i=1\\ P_{s,i-1}^{+}(z=L_{i-1},\nu_s,t)\beta_{i-1}C_{\rm out} & \dots\ \text{for } i=2\\ P_{s,i-1}^{+}(z=L_{i-1},\nu_s,t)\beta_{i-1} & \dots\ \text{for } i=3\end{cases}\\
P_{p,i}^{-}(z=L_i) &= P_{p0,i}^{-} \quad \dots \quad \text{for } i=1\text{–}3,\\
P_{\rm ASE,i}^{+}(z=0,\nu,t) &= \begin{cases} P_{\rm ASE,i}^{+}(z=L_i,\nu,t)(1-C_{\rm in})(1-C_{\rm out})F(\nu)\alpha_{va} & \\ \quad +P_{\rm ASE,i}^{-}(z=0,\nu,t)(1-C_{\rm in})\alpha_{\rm is} & \dots\ \text{for } i=1\\ P_{\rm ASE,i-1}^{+}(z=L_{i-1},\nu,t)\beta_{i-1}C_{\rm out} & \dots\ \text{for } i=2\\ P_{\rm ASE,i-1}^{+}(z=L_{i-1},\nu,t)\beta_{i-1} & \dots\ \text{for } i=3\end{cases}\\
P_{\rm ASE,i}^{-}(z=L_i,\nu,t) &= \begin{cases} P_{\rm ASE,i+1}^{-}(z=0,\nu,t)\beta_i C_{\rm out} & \dots\ \text{for } i=1\\ P_{\rm ASE,i+1}^{-}(z=0,\nu,t)\beta_i & \dots\ \text{for } i=2\\ 0 & \dots\ \text{for } i=3.\end{cases} \qquad (2)
\end{aligned}
$$

TABLE I
FIBER PARAMETERS USED IN NUMERICAL SIMULATIONS

fiber parameter	α [dB/km]		peak value of $g_R(\nu-\xi)/A_{eff}(\nu)$ [1/W/m]	
fiber typ	1480 nm	1550 nm	1420 nm	1510 nm
DCF	0.33	0.26	$2.384 \cdot 10^{-3}$	$1.961 \cdot 10^{-3}$

the total loss of the feedback loop, several tens of iterations are necessary to find steady-state power distributions along the cascade. In contrast with the numerical model presented in [18], our model takes into account propagation of both the downstream and upstream ASE spectral components and their temperature dependence. Moreover, only the first amplifier of the cascade is gain clamped, and the lasing power generated in the AOGC LRFA_1 propagates through the cascade.

Once the steady-state distribution of forward- and backward-propagating optical powers is calculated, direct integration according to (3) is used to obtain time evolution of individual optical powers $P^{\pm}(z,\nu,t)$ along the optical fiber in response to channel addition/removal. The time derivative $(\partial P^{\pm}(z,\nu,t))/(\partial t)$ is separated from (1).

$$P^{\pm}(z,\nu,t+\delta t) = P^{\pm}(z,\nu,t) + \frac{\partial P^{\pm}(z,\nu,t)}{\partial t} \cdot \Delta t. \quad (3)$$

To simulate channel loss/addition, the input power of some channels is 100% square-wave modulated with 50% duty cycle (see (4) shown at the bottom of the page), where $T_m = 1/f_m$ is the period of square-wave modulation. In order to avoid possible oscillations of the solution in the time domain, care must be taken in the selection of bin widths used in the space (Δz) and time (Δt) discretization schemes.

We will now present the results of numerical simulations performed with the same signal wavelengths, input powers, and VAT settings as used in the experiments shown in Figs. 3–6 ($\lambda_1 = 1545$ nm, $P_{s0}^{+}(1545\ \mathrm{nm}) = -8$ dBm, $\lambda_2 = 1550$ nm, $P_{s0}^{+}(1550\ \mathrm{nm}) = -1$ dBm, $\beta_1 = 9.5$ dB, and $\beta_2 = 14.2$ dB). The most important fiber parameters used in our simulations are summarized in Table I, peak values of the Raman gain coefficient $g_R(\nu-\xi)/A_{\mathrm{eff}}(\nu)$ are given at a pump wavelength of 1420 and 1510 nm, [21], and the wavelength dependence of the Rayleigh backscattering coefficient γ is considered in the form $\gamma(\lambda) = 2.3510^{-25}/\lambda^3$, [m^{-1}] [19]. Fig. 7 shows the steady-state gain-saturation characteristic of the LRFA_1. The net gain is plotted as a function of the input signal power at 1545 nm for the unclamped LRFA and two different clamping conditions $\alpha_l = 12$ and 10 dB (α_l is the total loss of the ring-laser loop). When the optical feedback loop is closed, the net gain is clamped to the value roughly equal to the total loop loss. For $\alpha_l = 12$ dB, the gain is clamped to 11.86 dB for an input power ranging from -35 to -2.5 dBm with a deviation less than 0.2 dB; for $\alpha_l = 10$ dB, the gain deviation is less than 0.04 dB within the input power ranging from -35 to $+2.0$ dBm.

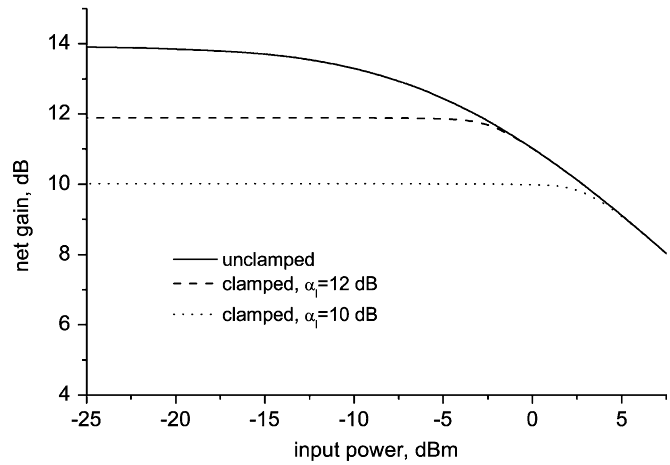

Fig. 7. Simulation: Single-channel (1545 nm) net gain of LRFA_1 as a function of the input signal power with and without AOGC. Loop loss: $\alpha_l = 10$ and 12 dB.

Fig. 8 depicts the net gain and optical signal-to-noise ratio (OSNR) of LRFA_1, LRFA_2, and LRFA_3 at 1545 and 1550 nm for the case in which the optical feedback loop of the LRFA_1 is open (dashed lines) and closed (full lines). The OSNR has been calculated with an ASE spectral resolution of 0.2 nm. For the gain-clamped case, the net gain does not change along the cascade, and the OSNR slightly deteriorates along the cascade (40 dB at the output of LRFA_1, and 37.5 dB at the output of LRFA_3). The decrease of the OSNR is more pronounced in case of the gain-clamped cascade. The effect of double Rayleigh scattering (DRS) on the performance of AOGC LRFA has been investigated. In order to assess the impact of DRS, the Rayleigh backscattering coefficient γ was set to zero. Fig. 9 compares the evolution of OSNR along the AOGC cascade for signals at 1545 and 1550 nm when the DRS was taken into account or disregarded. It can be concluded that due to the DRS, the OSNR of LRFA_1 decreases by 2.4 and by 3.6 dB at 1545 and 1550 nm,

$$P_{s0}^{+}(\nu_s,t) = \begin{cases} P_{s0}^{+}(\nu_s) & kT_m \le t < \left(k+\frac{1}{2}\right)T_m \qquad k=0,1,2,\ldots \\ 0 & \left(k+\frac{1}{2}\right)T_m \le t < (k+1)T_m \quad k=0,1,2,\ldots \end{cases} \quad (4)$$

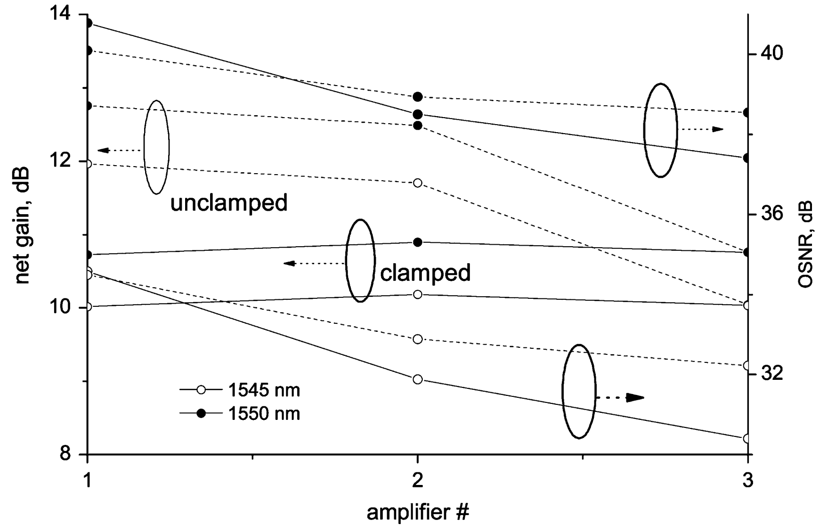

Fig. 8. Simulation: Net gain and OSNR of $\mathrm{LRFA}_1, \mathrm{LRFA}_2$, and LRFA_3 in the case in which the optical feedback loop of LRFA_1 is open and closed ($\alpha_l = 10$ dB).

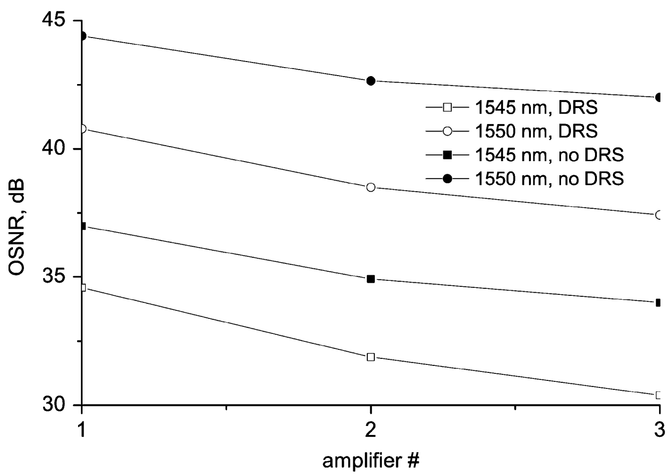

Fig. 9. Simulation: Evolution of OSNR along the cascade in case that the optical feedback loop of the LRFA_1 is closed ($\alpha_l = 10$ dB) and the Rayleigh backscattering is taken into account or disregarded.

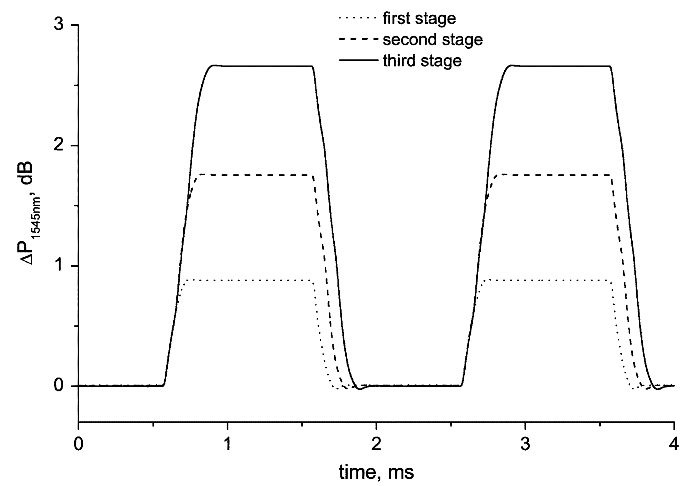

Fig. 10. Simulation: Output power variation of the 1545-nm signal at the output port of $\mathrm{LRFA}_1, \mathrm{LRFA}_2$, and LRFA_3 for the unclamped cascade.

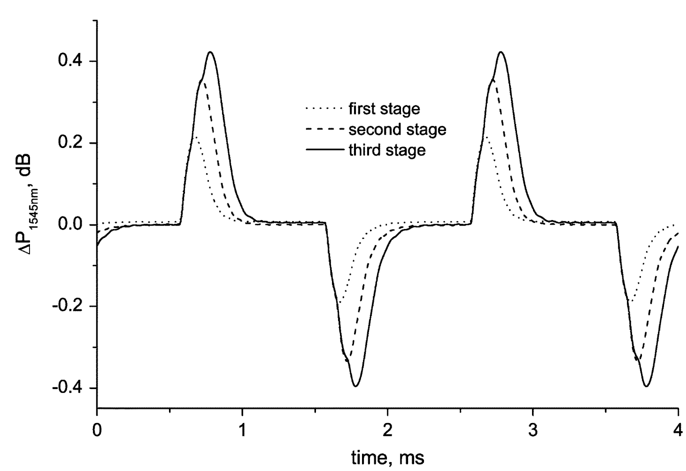

Fig. 11. Simulation: Output power variation of the 1545-nm signal at the output port of $\mathrm{LRFA}_1, \mathrm{LRFA}_2$, and LRFA_3 for the clamped cascade. $\alpha_l = 10$ dB.

respectively. The deterioration of the OSNR increase along the cascade.

Calculated power fluctuations of the 1545-nm signal channel after $\mathrm{LRFA}_1, \mathrm{LRFA}_2$, and LRFA_3 for the case of the unclamped cascade are shown in Fig. 10. The steady-state value of power fluctuations grows along the cascade in the same way as in the experimental results (see Fig. 3). The power undershoots recorded experimentally when the 1550-nm channel is added have not been obtained, although similar undershoots appeared in other results of numerical simulations (see [17, fig. 4]). Fig. 11 plots the time evolution of $\Delta P_{1545\mathrm{nm}}$ when the all-optical feedback loop is closed and $\alpha_l = 10$ dB. In this gain-clamped regime, the steady-state fluctuations are completely eliminated. Dynamic overshoots that occur when channels are dropped are about 7.5 dB lower than the corresponding steady-state power variations in the unclamped cascade. Peak values of the overshoots are 0.21, 0.35, and 0.42 dB, and the transients reach 10% of the peak value within 298, 355, and 427 μs after $\mathrm{LRFA}_1, \mathrm{LRFA}_2$, and LRFA_3, respectively. The corresponding undershoots are about 5% lower. Fig. 12 plots time variation of lasing power at the output port

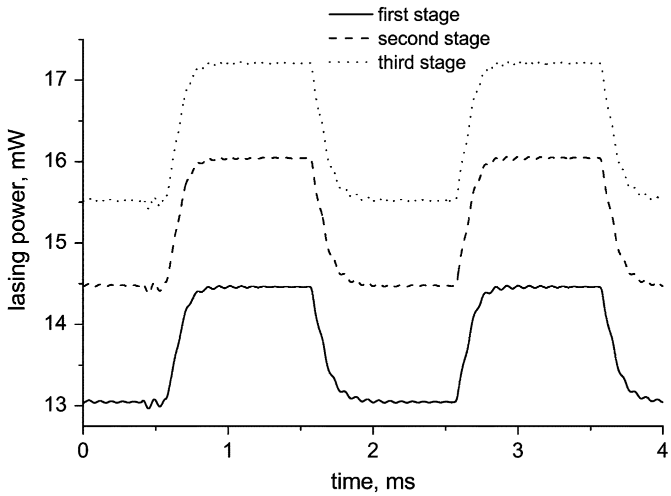

Fig. 12. Simulation: Time variation of lasing power at 1547 nm at the output of $\mathrm{LRFA}_1, \mathrm{LRFA}_2$, and LRFA_3. $\alpha_l = 10$ dB.

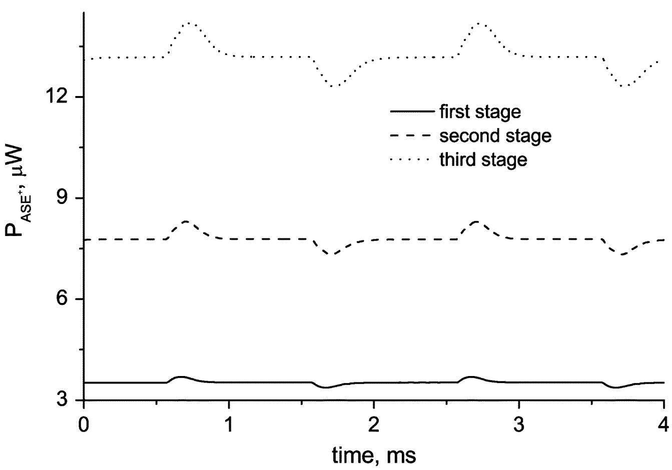

Fig. 13. Simulation: Time variation of downstream ASE power contained in a 1-nm slot centered at 1549 nm at the output of $\mathrm{LRFA}_1, \mathrm{LRFA}_2$, and LRFA_3. $\alpha_l = 10$ dB.

of individual LRFA's for $\alpha_l = 10$ dB. As expected, when channels are dropped, more gain is available, and the lasing power increases and reaches new steady-state value corresponding to the reduced input signal power. Transients of downstream ASE spectral components copy the surviving channel power transients. Fig. 13 shows the time evolution of ASE power contained in the 1-nm frequency slot centered at 1549 nm at the output of $\mathrm{LRFA}_1, \mathrm{LRFA}_2$, and LRFA_3. Steady-state ASE power at this wavelength grows along the cascade from 3.5 μW at the output of LRFA_1 to 13.2 μW at the output of LRFA_3.

IV. Conclusion

This paper described the investigation of suppression of power transients in a cascade of three lumped RFAs both theoretically and experimentally. The gain of the first LRFA was clamped using an optical feedback loop; the lasing power generated in the ring laser was propagated through the other two LRFAs. In these experiments, signals from two lasers were transmitted through the cascade. The light of one of the lasers was 100% square-wave modulated at 500 Hz to simulate channel addition/removal. The power fluctuations of the other signal caused by cross-gain modulation of the LRFAs were monitored at the output of individual amplifiers with a digital oscilloscope. It was found that when sufficient lasing in the AOGC LRFA_1 is allowed, steady-state power fluctuations are eliminated completely. The amplitude of the remaining power transients that occur when channels are switched off is about eight times lower than the steady-state power excursion of the unclamped cascade. The duration of these power transients is related to the length of the Raman fiber and the available pump power.

The theoretical analysis is based on an application of a numerical model that incorporates time variation effects in LRFA and can solve propagation equations for multiwavelength pumps, signals, and both the forward- and backward-propagating ASE powers. Boundary conditions for ASE spectral components of the AOGC LRFA_1 represent the ring-laser configuration. The wavelength dependence of fiber loss, Rayleigh backscattering, and group velocity are taken into account.

References

[1] Y. Sun, A. K. Srivastawa, J. L. Zyskind, C. Wolf, J. W. Sulhoff, and R. W. Tkach, "Fast power transients in WDM optical networks with cascaded EDFAs," *Electron. Lett.*, vol. 33, pp. 313–314, Feb. 1997.

[2] A. K. Srivastava, Y. Sun, J. L. Zyskind, and J. W. Sulhoff, "EDFA transient response to channel loss in WDM transmission system," *IEEE Photon. Technol. Lett.*, vol. 9, pp. 386–388, Mar. 1997.

[3] J. L. Zyskind, A. K. Srivastava, Y. Sun, J. C. Ellson, G. W. Newsome, R. W. Tkach, A. R. Chraplyvy, J. W. Sulhoff, T. A. Strasser, J. R. Pedrazzani, and C. Wolf, "Fast link control protection for surviving channels in multiwavelength otical networks," in *Proc. Eur. Conf. Optical Communications*, Oslo, Norway, 1996. Paper ThC.3.6.

[4] J. C. van der Plaats, F. W. Willems, and A. M. J. Koonen, "Dynamic pump-loss controlled gain-locking system for erbium-doped fiber amplifiers in multi-wavelength networks," in *Proc. Eur. Conf. Optical Commununications*, Edinburgh, U.K., 1997.

[5] M. Karasek and F. W. Willems, "Suppression of dynamic cross saturation in cascades of overpumped erbium-doped fiber amplifiers," *IEEE Photon. Technol. Lett.*, vol. 10, pp. 1036–1038, July 1998.

[6] E. Delevaque, T. Georges, J. F. Bayon, M. Monerie, P. Niay, and P. Berage, "Gain control in erbium-doped fiber amplifiers by lasing at 1480 nm with photoinduced Bragg gratings written on the fiber ends," *Electron. Lett.*, vol. 29, pp. 1112–1114, 1993.

[7] J. F. Massicott, S. D. Willson, R. Wyatt, J. R. Armitage, R. Kashyap, and D. Williams, "1480 nm pumped erbium doped fiber amplifier with all-optical automatic gain control," *Electron. Lett.*, vol. 30, pp. 962–964, 1994.

[8] H. Dai, J. Y. Pan, and Ch. Lin, "All-optical gain control of in-line erbium-doped fiber amplifiers for hybrid analog/digital WDM systems," *IEEE Photon. Technol. Lett.*, vol. 9, pp. 737–739, June 1997.

[9] S. Y. Kim, J. Chung, and B. Lee, "Dynamic performance of the all-optical gain-controlled EDFA cascade in multiwavelength optical networks," *Electron. Lett.*, vol. 33, pp. 1475–1477, Aug. 1997.

[10] G. Luo, J. L. Zyskind, Y. Sun, A. K. Srivastava, J. W. Sulhoff, C. Wolf, and M. A. Ali, "Performance degradation of all-optical gain-clamped EDFA's due to relaxation-oscillations and spectral-hole burning in amplified WDM networks," *IEEE Photon. Technol. Lett.*, vol. 9, pp. 1346–1348, Oct. 1997.

[11] C. J. Chen and W. S. Wong, "Transient effects in saturated Raman amplifiers," *Electron. Lett.*, vol. 37, pp. 371–373, Mar. 2001.

[12] M. Karasek and M. Menif, "Channel addition/removal response in Raman fiber amplifiers: Modeling and experimentation," *J. Lightwave Technol.*, vol. 20, pp. 1680–1687, Sept. 2002.

[13] C. J. Chen, J. Ye, W. S. Wong, Y. W. Lu, M. C. Ho, Y. Cao, M. J. Gassner, J. S. Pease, H. S. Tsai, H. K. Lee, S. Cabot, and Y. Sun, "Control of transient effects in distributed and lumped Raman amplifiers," *Electron. Lett.*, vol. 37, pp. 1304–1306, Oct. 2001.

[14] M. Karasek and M. Menif, "Protection of surviving channels in pump-controlled gain-locked Raman fiber amplifier," *Optics Communications*, vol. 210, pp. 57–65, 2002.

[15] S. S.-H. Yam, F.-T. An, E. S.-T. Hu, M. E. Marhic, T. Sakamoto, L. G. Kazovsky, and Y. Akasaka, "Gain-clamped S-band discrete Raman amplifier," in *Proc. Optical Fiber Communication Conf. (OFC'02)*, 2002, pp. 385–387. Paper ThB4 385.

[16] G. Sacchi, S. Sugliani, B. Bolognini, S. Faralli, and F. DiPasquale, "Experimental analysis of gain clamping techniques for lumped Raman amplifiers," in *Proc. Eur. Conf. Optical Communication (ECOC'03)*, 2003, pp. 226–227. Paper Tu3.2.4.

[17] M. Karasek, J. Kanka, P. Honzatko, and J. Radil, "Protection of surviving channels in all-optical gain-clamped Raman fiber amplifier: Modeling and experimentation," *Optics Communications*, vol. 231, pp. 309–317, 2004.

[18] B. Bolognini and F. DiPasquale, "Transient effects in gain-clamped discrete Raman amplifier cascades," *IEEE Photon. Technol. Lett.*, vol. 16, pp. 66–68, Jan. 2004.

[19] H. Kidorf, K. Rottwitt, M. Nissov, M. Ma, and E. Rabarijaona, "Pump interactions in a 100-nm bandwidth Raman amplifier," *IEEE Photon. Technol. Lett.*, vol. 11, pp. 530–532, May 1999.

[20] C. J. Chen, H. Lee, and Y. J. Cheng, "Instability in Raman amplifiers caused by distributed Rayleigh reflection," in *Proc. Optical Fiber Communications Conf. (OFC2003)*, vol. 1, Atlanta, GA, 2003. Paper TuC2.

[21] S. Namiki and Y. Emori, "Ultrabroad-band Raman amplifiers pumped and gain-equalized by wavelength-division-multiplexed high-power laser diodes," *IEEE J. Select. Topics Quantum Electron.*, vol. 7, pp. 3–16, Jan./Feb. 2001.

M. Karásek received the Ing. degree (honors) from the Czech Technical University, Prague, Czech Republic, in 1969 and the Ph.D. degree in microwave semiconductor devices and the Doctor of Sciences degree from the Institute of Radio Engineering and Electronics (IREE), Academy of Sciences of the Czech Republic, Prague, Czech Republic, in 1974 and 1990, respectively.

He is currently a Senior Researcher at the IREE. His research activities are in the area of measurement and computer modeling of active fibers for fiber lasers and fiber amplifier applications and in the area of optical communications.

J. Kaňka, photograph and biography not available at the time of publication.

Jan Radil was born in Prague, Czech Republic. He received the M.Sc. and Ph.D. degrees in electrical enginnering from the Czech Technical University, Prague, Czech Republic, in 1996 and 2004, respectively.

He joined the Research and Development Department, CESNET, Prague, Czech Republic, in 1999, where he is responsible for optical networking and development of the next generation of the Czech research and educational network.